*Journal of Applied Fluid Mechanics*, Vol. 19, No. 1, pp. 3297-3311, 2026. Available online at <a href="https://www.jafmonline.net">www.jafmonline.net</a>, ISSN 1735-3572, EISSN 1735-3645. <a href="https://doi.org/10.47176/jafm.19.1.3606">https://doi.org/10.47176/jafm.19.1.3606</a>



### Design and Research for a Gas-water Separator for Pump Cavitation Testing

S. Y. Dong<sup>1</sup>, J. G. Mou<sup>1†</sup>, B. Xiong<sup>2</sup>, X. H. Liu<sup>1</sup>, Y. X. Yang<sup>3</sup>, S. N. Fan<sup>3</sup> and Z. K. Liu<sup>3</sup>

<sup>1</sup> College of Metrology Measurement and Instrument, China Jiliang University, Hangzhou 310018, China
<sup>2</sup> Eifel Pump (Fuzhou) Corpn, Ltd, Fuzhou 350101, China
<sup>3</sup> College of Energy Environment and Safety Engineering, China Jiliang University, Hangzhou 310018, China

†Corresponding Author Email: mjg@cjlu.edu.cn

#### **ABSTRACT**

In open-type cavitation tests, pump inlet air bubbles affect the accuracy of cavitation margin measurements. To improve the accuracy of these measurements, a novel gas-water separation device for pump cavitation testing was designed in this study based on the principle of multiphase flow separation. This device could effectively remove unintended air bubbles. Through numerical simulations and experimental studies, we characterized the internal flow field features and quantified how the inner cylinder length-to-diameter ratio governed the separation efficiency and pressure drop, finding an optimal lengthto-diameter ratio of 2.5 for maximum gas removal. The shape of the inner cylinder and the outlet structure was optimized, and the large curvature (LC) structure minimized a pressure loss of 314.6 Pa while maximizing the separation efficiency to 89.66%. The degrees of influence exerted by the internal cylinder diameter at the bottom, the internal cylinder inclination, and the internal cylinder height on the separation performance of the LC structure were investigated through orthogonal tests. The bottom diameter of the internal cylinder was found to have the most significant influence. These results offer practical guidance for enhancing cavitation-test accuracy and informing the optimal design of gaswater separators.

### Article History

Received April 21, 2025 Revised July 18, 2025 Accepted August 8, 2025 Available online November 5, 2025

#### Keywords:

Multiphase flow Gas-water separation Cavitation test Structure design Numerical simulation

### 1. Introduction

Pumps serve as critical energy conversion devices across sectors such as aerospace, nuclear power, and agricultural irrigation (Qiaorui et al., 2023; Ji et al., 2023). However, the performance and operational safety of these types of pumps are often compromised by cavitation (Jiegang et al., 2020; Guixuan et al., 2023; Bo et al., 2024), which is a complex multiphase flow phenomenon involving gas—liquid phase changes (Li et al., 2022; Gu et al., 2022).

Cavitation occurs when the local pressure falls below the liquid vapor pressure, causing bubble growth. These cavities then collapse downstream under higher pressure, producing intense shock waves and high-frequency pressure pulses (Lu et al., 2022). Thousands of these types of collapse events can erode impeller surfaces, trigger vibrations, and noise, and the collapse events pose substantial risks to pump integrity (Tan et al., 2023; Sakran et al., 2022; Ma et al., 2022).

Because net positive suction head (NPSH) cannot be fully predicted by theory, centrifugal pumps are factory tested with step-wise reduced inlet pressure until a 3% head-drop indicates cavitation onset (Xiaoqi et al., 2023; Rudolf et al., 2010). However, this method often induces cavitation at the control valve due to the sudden pressure drop and increased local velocity, and bubbles are generated that may not collapse before entering the pump, which skews the test results (Yongbing et al., 2020). Consequently, the incorporation of a gas—water separator between the valve and the pump inlet has been recommended to remove these early-forming bubbles and ensure measurement accuracy (Jorge et al., 2024).

In recent years, researchers have conducted extensive studies on gas-water separation technology, achieving notable progress in various domains.

These progress areas include research on the separation mechanism, flow field characteristics, and structure optimization. Zheng et al. (2019) proposed a new kind of gas—liquid separator to separate gas—liquid mixtures for different flow patterns. The experimental

results showed that the separator could enable highly efficient separation. Jincheng et al. (2023) investigated internal velocity distribution, pressure distribution, and separation efficiency, which provided a specific reference for the design of an axial flow cyclone separator. Hreiz et al. (2011) investigated the effect of inlet geometry on cyclone hydrodynamics and found that a rectangular inlet performed better than a circular one. The study conducted by Yan-ria et al. (2012) demonstrated that enhancing the length of the cylinder and the diameter of the outlet pipe while maintaining optimal proportions could lead to a substantial enhancement in the stability of the separator.

Recent CFD studies have further quantified how geometric parameters govern separator performance. For instance, Mao et al. (2024) conducted CFD simulations on axial-flow cyclone separators and found that increasing the blade count, adjusting the blade exit angle, and enlarging the vortex-finder and exhaust-pipe diameters significantly improved the tangential velocity and separation efficiency, though at the expense of increased pressure drop. Similarly, the mini-hydro cyclone simulations by He et al. (2022) revealed that deepening the vortex finder expanded the pre-separation zone but increased energy consumption. The researchers identified an optimal  $L_0/D$  ratio of approximately 1.0. Pandey et al. (2022) examined the impact of different cone and cylinder heights on the performance of cyclone separators utilizing CFD simulation. The researchers found that convex cones minimized pressure loss while straight cones maximized separation efficiency, and longer cylindrical sections consistently reduced pressure drop with only minor efficiency penalties.

These numerical results demonstrated that, based on computational fluid dynamics (CFD), the optimization of the structural parameters of a separator could quantitatively improve separation efficiency, reduce the pressure drop, stabilize the flow field, and effectively manage the pressure loss. However, most studies have targeted oil—water or gas—solid systems, with few explicitly addressing water pump cavitation applications (Zhi et al., 2024).

To address this deficit, a novel gas—water separator is proposed in this paper. This gas—water separator was specifically designed for the purpose of water pump cavitation tests. The device was studied utilizing numerical simulation to analyze the internal flow field characteristics, and the effect of the gas—water separation device was verified through experiments. An investigation was conducted on the impact of different inner cylinder length-to-diameter ratios on the separation performance. Orthogonal tests were used to determine the degree of influence of various factors on the separation performance.

# 2. SIMULATION ANALYSIS AND EXPERIMENTAL VALIDATION OF THE GAS—LIQUID SEPARATOR

# 2.1 Separation Mechanism of the Gas-Water Separator

The function of a gas-water separator is based on the mutual incompatibility of gas and water and their

differences in density and gravity (Fig. 1). When the valve opening is adjusted, bubbles are created in the water flow, and these bubbles then enter the separator and inner cylinder, where the flow rate slows down. After the mixtures flow out of the cylinder, the liquid flows into the pump, and the gas is discharged. This reduces the number of bubbles in the pump and ensures the accuracy of the test.

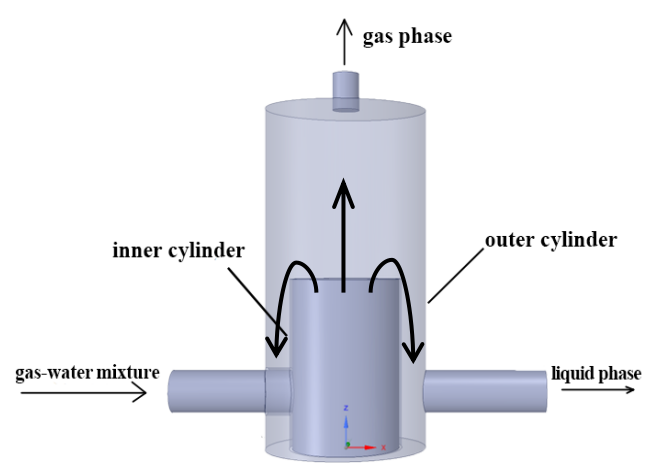


Fig. 1 Separation principle of air-water separator

The separation device consisted of five parts: the inner cylinder, the outer cylinder, the bottom flow outlet, the gas phase outlet, and the mixture inlet. Design experience with other separators, such as gas—liquid cylindrical cyclone and axial-flow separators, was utilized for reference (Zhen et al., 2022; Rui et al., 2019; Mengyang et al., 2023). The outer cylinder was cylindrical, the inlet cross-section was circular, a single inlet was connected to the inner cylinder, and the gas phase outlet tube was cylindrical. The initial structural parameters of the gas—water separator are shown in Fig. 2 and Table 1.

Table 1 Values of initial structural parameters

Structural parameters	Symbol	Value
Diameter of outer cylinder	D	300
Diameter of inner cylinder	d	150
Height of outer cylinder	H	600
Height of inner cylinder	h	325
Inlet tube diameter	$d_{I}$	75
Bottom flow outlet diameter	$d_2$	75
Gas phase outlet diameter	d3	50
Length of gas phase outlet	l	65
Length of inlet pipe, bottom flow outlet	L	225
Thickness of the wall	δ	5
Bottom flow outlet diameter	θ	75
Height of inlet pipe, bottom flow outlet from the bottom surface	h'	100

#### 2.2 Cavitation Test Verification

According to the designed structure, the separator test prototype was machined. A physical diagram of the separator is shown in Fig. 3. The Q-NPSH curve (Fig. 4) shows that after the addition of the separator, the NPSH decreased and the NPSH difference increased with increasing

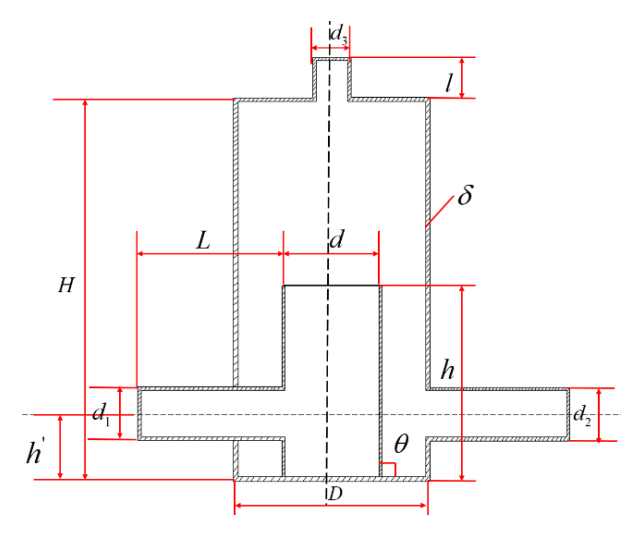
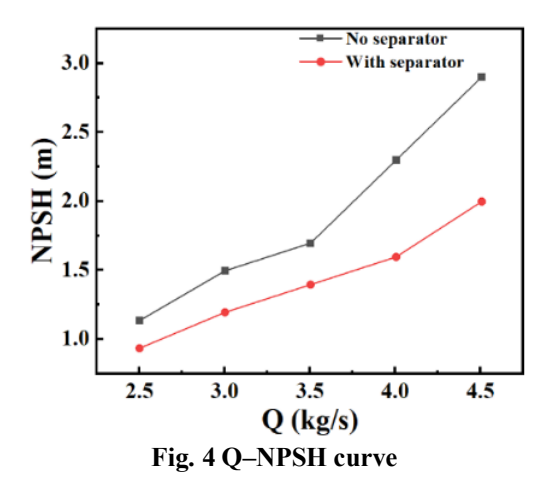


Fig. 2 Basic structure of gas-water separator



Fig. 3 Separator prototype



flow rate, indicating that the separator could effectively separate the air bubbles and improve the accuracy of the cavitation test. At the same time, after the addition of the separator, the water flow at the pump inlet was smooth, proving that the separator had a stabilizing effect on the flow.

## 2.3 Numerical Modeling and Grid Independence Verification

The physical model was created using SolidWorks. Since the model in this study needed to be replaced

continuously and the inner cylinder had a wall thickness that needed to be taken into consideration, Fluent Meshing was selected for the unstructured mesh generation. The mixing model was selected as the multiphase flow separation model, the RNG  $k-\varepsilon$  model was selected as the turbulence model, the velocity inlet was used for the inlet, the outflow was used for the outlet boundary condition, the wall was set as the no-slip boundary condition, and the QUICK format and SIMPLEC algorithm were selected.

The grid number affected computational accuracy and speed, so grid independence verification was carried out before computation. As shown in Fig. 5, five different numbers of grids were simulated, and it was found that after Case 3 (with 544,521 grids), the separation efficiency and pressure drop did not change significantly. Therefore, Case 3 was selected for subsequent analysis.

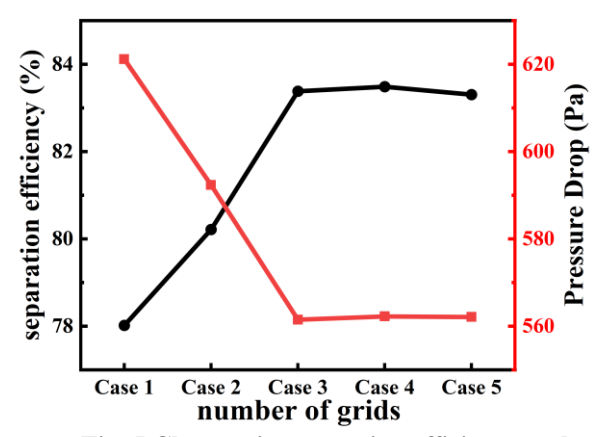


Fig. 5 Changes in separation efficiency and pressure drop for different numbers of grids

Figure 6 shows the mesh distribution generated by ANSYS Fluent Meshing with 544,521 grids. Local mesh refinement using BOI was applied to three critical regions: the model inlet, the bottom flow outlet, and the inner-cylinder upper outlet. Figure 7 shows a zoomed-in view of the outlet–cylinder junction. The figure reveals a hexdominant mesh and denser cell packing within the BOI zones to better capture complex flow gradients.

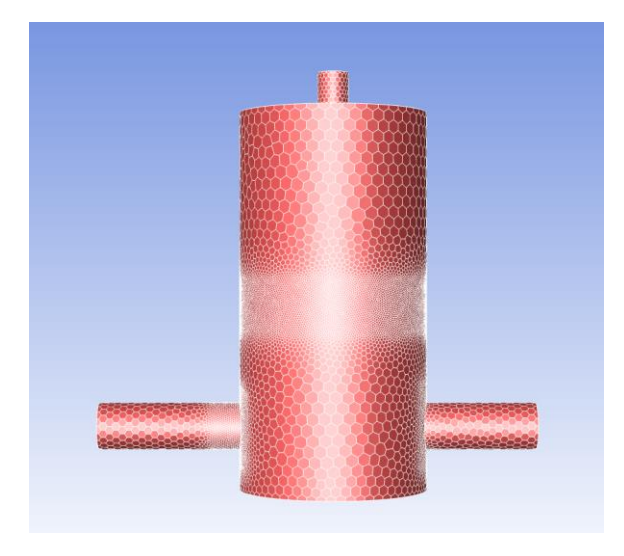


Fig. 6 Global mesh distribution

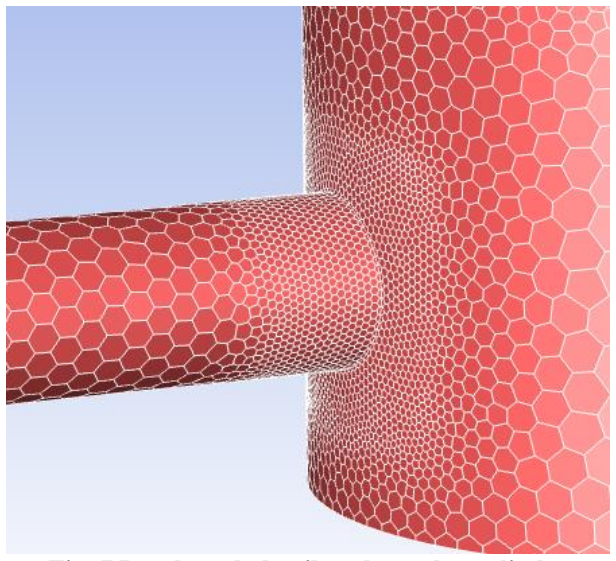


Fig. 7 Local mesh detail at the outlet-cylinder junction

### 2.4 Velocity Field and Pressure Field Distribution

In Fig. 8, the local vortex is illustrated in the red box. This local vortex may have resulted in energy loss. Figure 9 shows a velocity vector near the outlet of the inner cylinder, where, of the five primary vortices, 1–4 were close to the inner cylinder wall and 5 was close to the outer cylinder wall. The arrow directions show that the bottom flow outlet, inlet, and gas phase outlet were free of backflow and swirling flow, and the flow velocity distribution at the bottom flow outlet was more uniform. This suggests that the device played a rectification role and optimized the flow field. Reducing the local vortices also reduced energy losses, moderate cyclonic flow contributed to separation, and the rectification effect improved the separation efficiency and flow stability.

As shown in Fig. 10, the axial, radial, and tangential velocities were symmetrically distributed. The curve in the figure breaks at a radial position of 75 mm because this position corresponds to the inner cylinder wall thickness, and the data were not available. In addition, all three velocities together affected the gas—water separation. The radial velocity had the smallest value but drove the bubble inwards. The axial velocity drove the gas up. The tangential velocity determined the acceleration within the device and affected the energy loss and separation efficiency.

The change in the tangential velocity mainly occurred in the inner cylinder. As shown in Fig. 10(a), the tangential velocity of the outer cylinder was close to 0 m/s, and there was no swirling flow generation. The central tangential velocity started to decrease at 125 mm and fell to 0 m/s at 200 mm, indicating that the strength of the swirling flow field was weakening. Above 200 mm, the velocity changed direction and increased slowly. Tangential velocity is a key factor in gas—water separation. If the inner cylinder is too long, it may lead to insufficient tangential velocity, triggering gas—liquid re-mixing and reducing the separation efficiency. Therefore, optimizing the height of the inner cylinder could improve the separation efficiency and reduce energy losses.

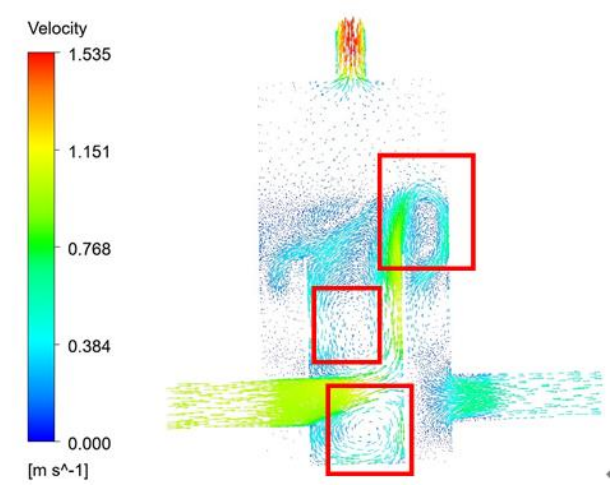


Fig. 8 Speed vector at X=0 mm

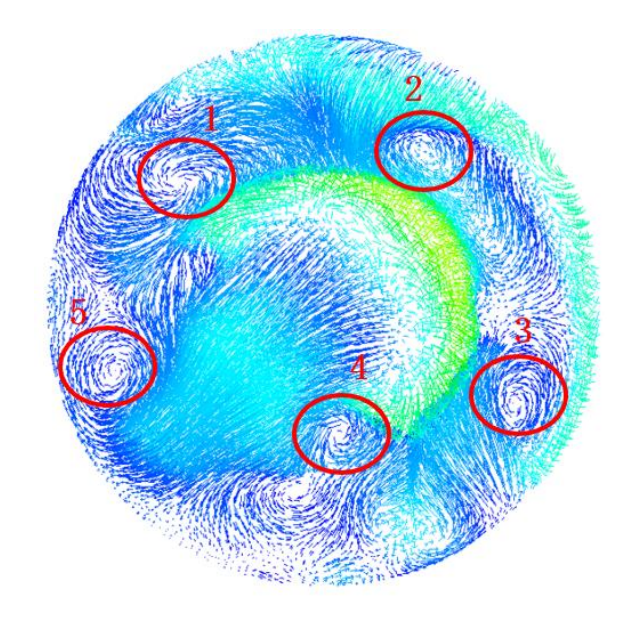


Fig. 9 Speed vector at Z=340 mm

In Fig. 10(b), in the region Z=50-125 mm, the axial velocity within the inner cylinder remained low, with a maximum value of approximately 0.5 m/s. By contrast, in the Z=150-275 mm section, the axial velocity increased significantly, reaching approximately 0.9 m/s near the cylinder wall, while the velocity along the central axis remained nearly zero. These zero-velocity points formed a closed surface, known as the axial zero-velocity envelope.

As shown in Fig. 10(c), at Z=50 and 75 mm, the radial velocity values on the left side of the outer cylinder (radial -75-0 mm) were positive, with a maximum of approximately 0.1 m/s. At the Z=100, 125, and 150 mm cross-sections, the radial velocity values in the same region were negative, with the maximum radial velocity occurring at Z=125 mm.

The contour map of the total pressure (Fig. 11) illustrates that the total pressure was at a maximum at the inlet tube and the bottom of the separator, and the total pressure gradually decreased along the axial direction. This indicated energy loss during the flow. The static pressure decreased axially and was greater at the inlet than

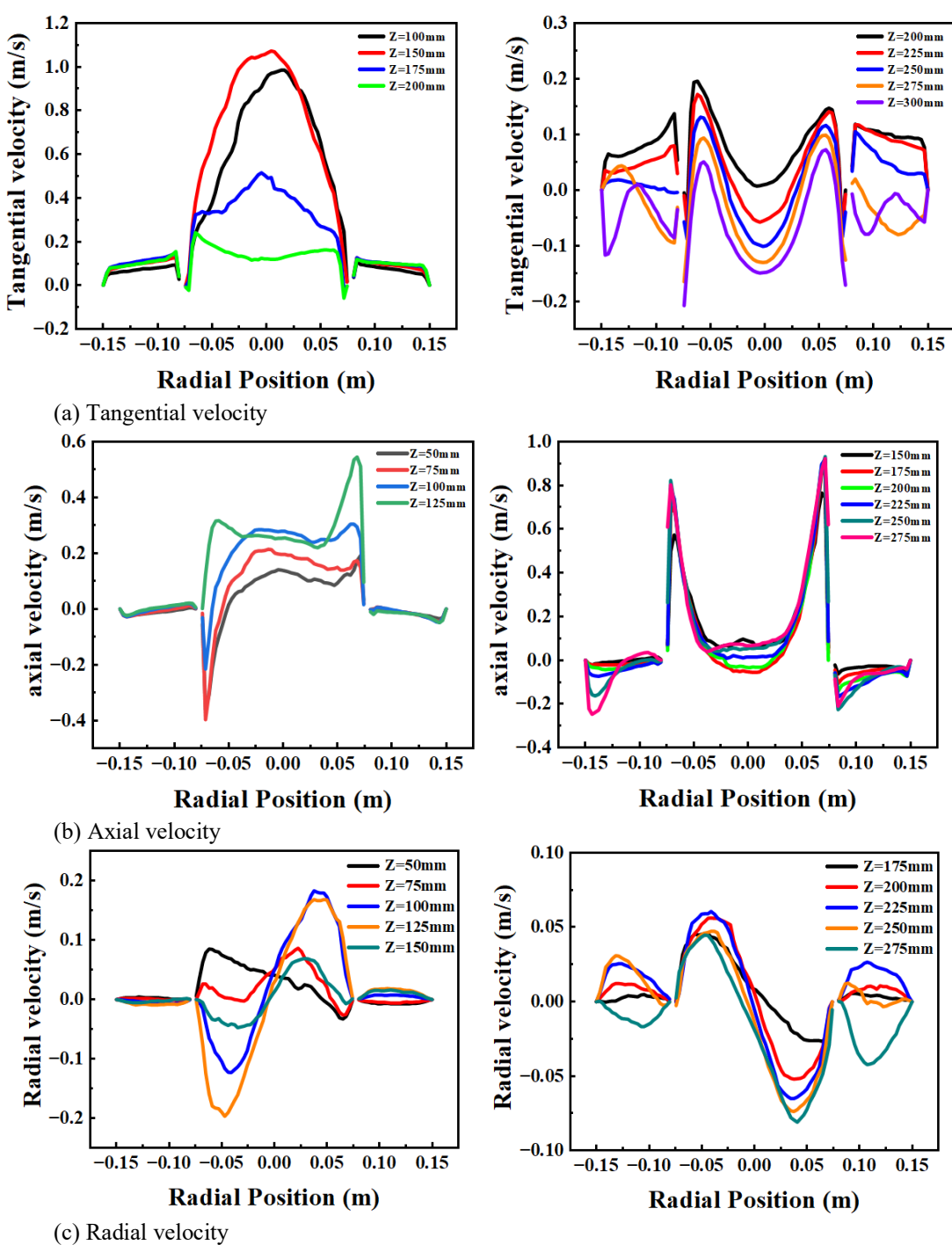


Fig. 10 Velocity distributions of each cross-section

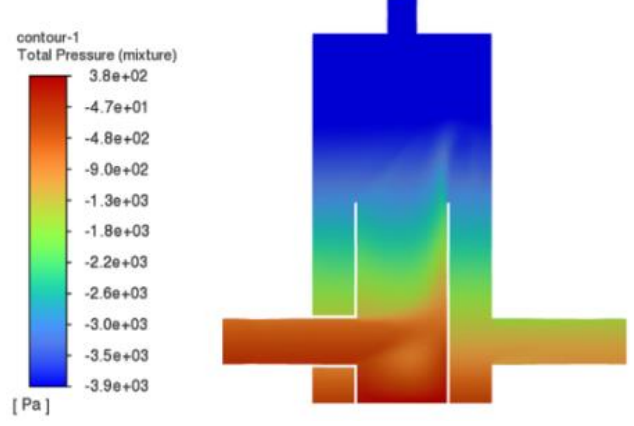


Fig. 11 Contour map of the total pressure

at the bottom flow outlet and gas phase outlet. This indicated that the gas—liquid separation was accompanied by energy loss. Consequently, the subsequent optimized design had to reduce the pressure loss and improve the separation efficiency and system stability.

### 2.5 Turbulent Kinetic Energy Distribution

The contour map (Fig. 12) shows the distribution of the turbulent kinetic energy inside the separator. The kinetic energy was stable with insignificant changes at the inlet tube, the bottom end of the inner cylinder, and the bottom flow outlet, while the turbulent kinetic energy increased significantly at the inner cylinder outlet and the gas phase outlet. This suggested enhanced flow perturbation in the gas phase outlet region, which may

Group number	1	2	3	4	5	6	7	8	9	10	11
Height of inner cylinder	300	300	300	300	300	275	325	350	375	400	450
Diameter of inner cylinder	200	175	150	125	100	150	150	150	150	150	150
Length-to-diameter ratio	1.50	1.71	2.00	2.40	3.00	1.83	2.17	2.33	2.50	2.67	3.00

Table 2 Parameter table for different length-to-diameter ratios

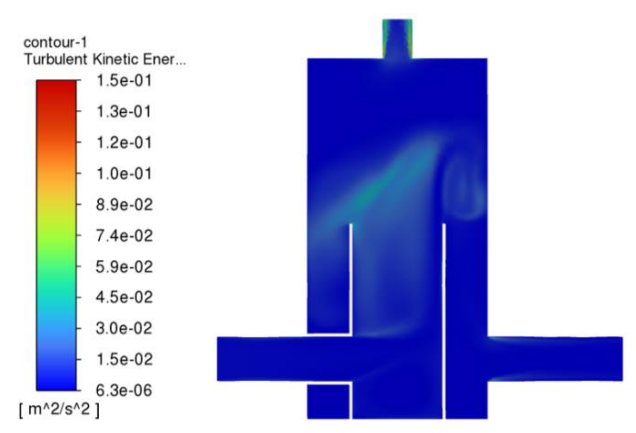


Fig. 12 Distribution of turbulent kinetic energy

have led to increased droplet entrainment and reduced separation efficiency. Therefore, optimizing the inner cylinder outlet structure reduced the turbulent kinetic energy and improved separation efficiency.

# 3. INFLUENCE OF LENGTH-TO-DIAMETER RATIO ON SEPARATION PERFORMANCE

Stabilizing the gas phase in the separator was a challenging process, and the gas phase had a comparatively brief residence time. The feasibility of achieving separation during the gas phase's residence time was contingent on the height of the inner cylinder. The quantity of gas transported by the bottom flow outlet was dependent on the inner cylinder diameter. Optimizing the parameters could mitigate gas accumulation. Furthermore, the cylinder's height functioned as a buffer for the water, facilitating the ascent of the bubbles. Modifying the separator's structural parameters, such as height and inner cylinder diameter, could enhance its separation efficiency and internal stability (Feiran et al., 2020; Chunyu et al., 2023). Optimizing the ratio of length to diameter for the inner cylinder also improved performance.

This section describes the optimization of the gas—water separator based on the parameters set in Section 3 (Table 2). Eleven groups of different length-to-diameter ratios were set (Group 7 was the initial parameter). The best ratio was determined by comparing its impact on performance. The inner cylinder height was fixed at 300 mm for the initial five groups, while the inner cylinder diameter was adjusted. Conversely, for Groups 6–11, the inner cylinder diameter was fixed at 150 mm, with the inner cylinder height being the variable factor.

### 3.1 Influence of Length-to-Diameter Ratio or Separation Efficiency

In Fig. 13, the YZ plane's liquid phase distribution contour map for 10 groups is shown, excluding Group 7.

The distribution was essentially unchanged, with more liquid to the right of the bottom outlet due to pressure and inertial force as the liquid flowed out of the inner cylinder. The elevated gas phase content at the bottom flow outlets of Groups 1 and 2 (in the blue circles) suggested low separation efficiency. The inner cylinder's diameter decreased in Groups 3–5, the distance between the cylinders increased, the space for separation became more extensive, and therefore the gas phase at the bottom of the flow outlet decreased.

The gas phase was more pronounced at the bottom flow outlets (in the black box) of Groups 6 and 8 and less so in Groups 9–11. However, the inner cylinder of Group 11 was taller, and there was less space for the air layer above the separator, which was not conducive to separation, resulting in a higher gas phase outlet liquid carryover rate. As shown in Fig. 14, the smallest gas mass flow rate of the gas phase at the bottom flow outlet of Group 3 was found to be  $-2.96 \times 10^{-5}$  kg/s, and the highest gas mass flow rate of the gas phase at the gas phase outlet was  $-4.38 \times 10^{-7}$  kg/s. This indicated that the gas bubbles rose smoothly for the diameter of the inner cylinder in Group 3.

Concurrently, Group 3 demonstrated the highest separation efficiency when the height of the inner cylinder was fixed. This finding suggested that the optimal inner cylinder diameter was 150 mm. An inner cylinder diameter that was too wide would result in insufficient space between the inner and outer cylinder walls. This would not be conducive to the rise of the bubbles and the separation of the water. Furthermore, an insufficiently small inner cylinder diameter would result in a diameter of the inlet pipe that was similar in size, which would not be conducive to the flow of fluids. The bottom flow outlet gas phase flow rate of Group 9 was second only to that of Group 3, which was  $-2.88 \times 10^{-5}$  kg/s. Furthermore, Group 9 demonstrated the maximum separation efficiency at a fixed height of the inner cylinder, which was higher than that of Group 3, reaching 87.63% (Fig. 15). It was evident that the separation efficiencies of Groups 3 and 9 were the two highest among the 11 groups.

# 3.2 Influence of Length-to-Diameter Ratio on Pressure Drop

The magnitude of the pressure drop at the bottom flow outlet indicated the energy consumption of the gas and liquid phases subsequent to their passage through the separator. As illustrated in Fig. 16, when the height of the inner cylinder was fixed, the diameter of the inner cylinder decreased, and the pressure drop initially decreased and subsequently increased. The large inner cylinder diameter left less space between the inner and outer cylinder walls, causing friction and energy dissipation when the fluid

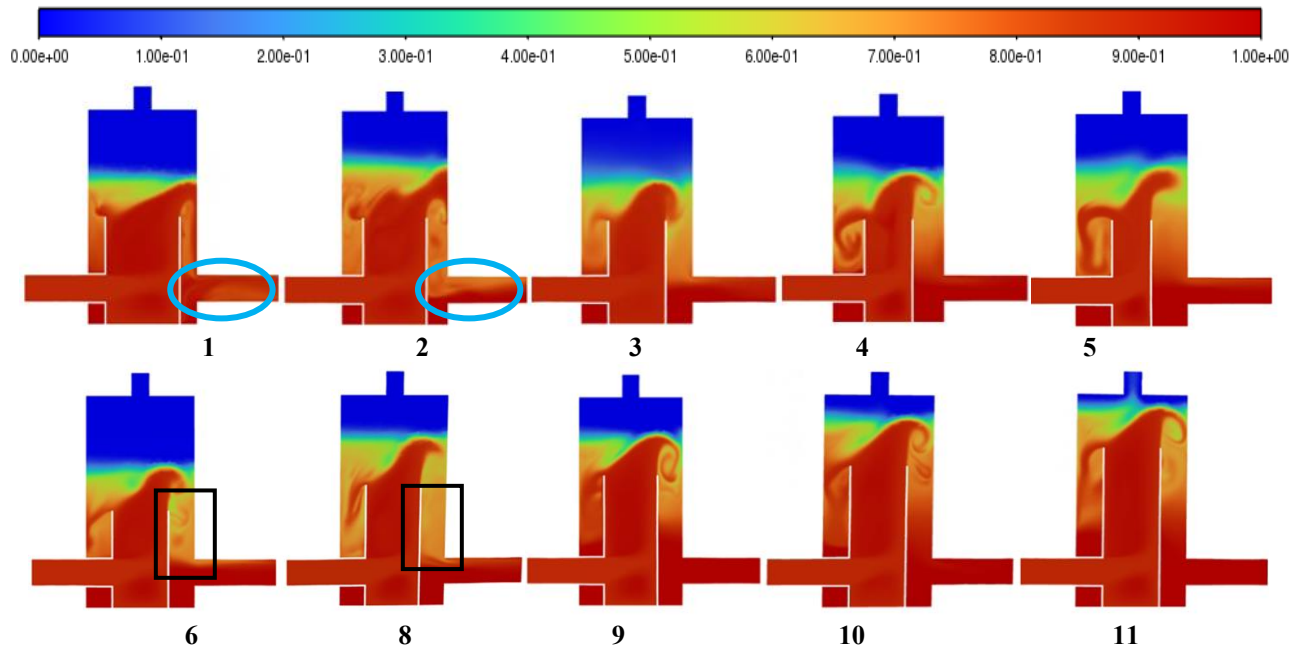


Fig. 13 Contour map of liquid phase distribution for different length-to-diameter ratios

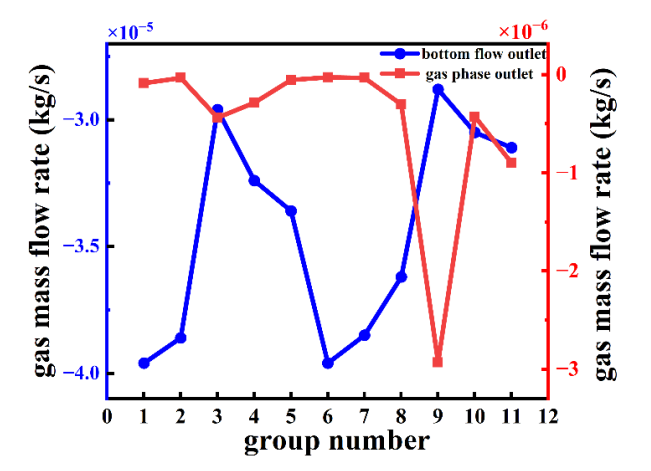


Fig. 14 Gas mass flow rate of the gas phase

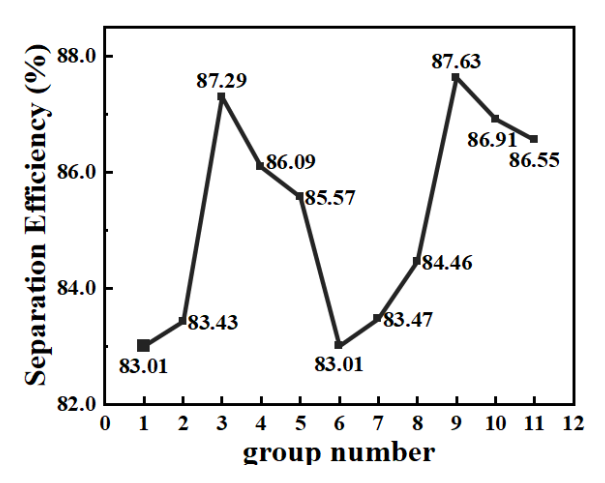


Fig. 15 Separation efficiency

flowed through. When the diameter of the inner cylinder was fixed, a higher inner cylinder height led to a lower pressure drop at first. Group 10 had the lowest pressure drop, showing that this height could reduce energy loss. At 450 mm, the pressure drop suddenly increased to 593.79 Pa.

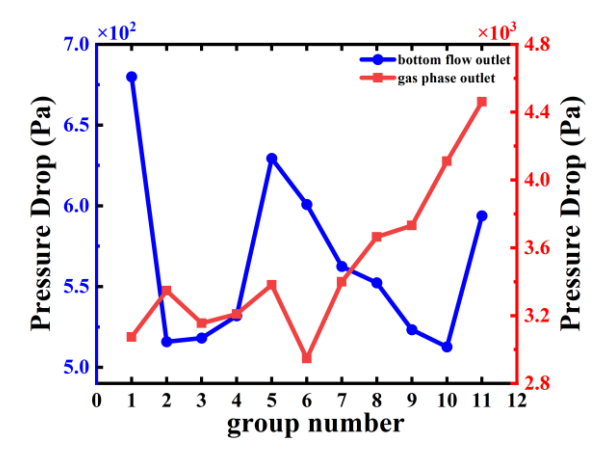


Fig. 16 Pressure drops for different length-todiameter ratios

Consequently, an appropriate increase in the height of the inner cylinder increased the time gas—liquid two-phase separation, thereby facilitating gas—liquid separation. However, if the height were excessively increased, it could readily trigger vortex flow and increase energy consumption. Group 6 had the lowest gas phase outlet pressure drop of 2947.19 Pa, but the bottom flow outlet pressure drop was high, and the separation efficiency was low. This suggested that Group 6 was not the optimum length-to-diameter ratio. Groups 2, 3, 4, 9, and 10 had similar bottom flow outlet pressure drop values, with the highest gas phase pressure drop for Group 10 at 4109.94 Pa, followed by 3731.03 Pa for Group 9.

The analysis of the separation efficiency and pressure drop indicated that, following adjustment of the length-to-diameter ratio of the inner cylinder, Groups 3, 9, and 10 exhibited optimal performance, with Group 9 demonstrating the highest separation efficiency.

Given the primary objective of reducing the gas content at the bottom flow outlet, priority had to be accorded to the separation efficiency, with the weights for

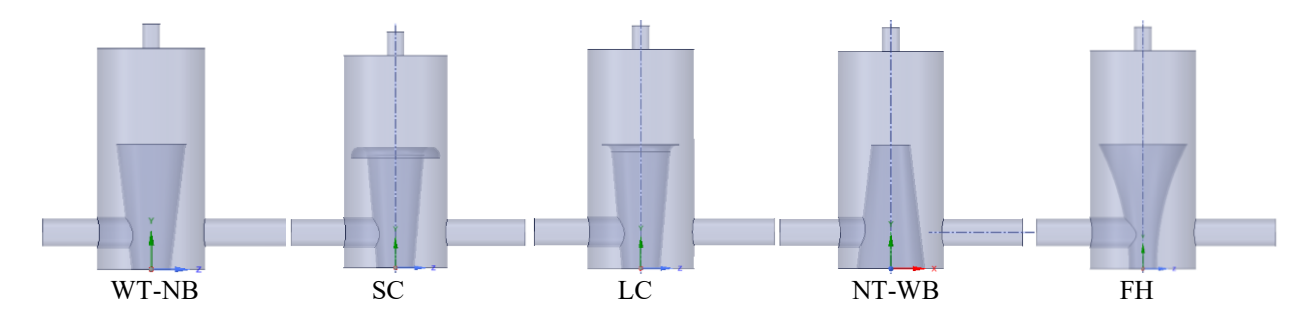


Fig. 17 Five different inner cylinder formats

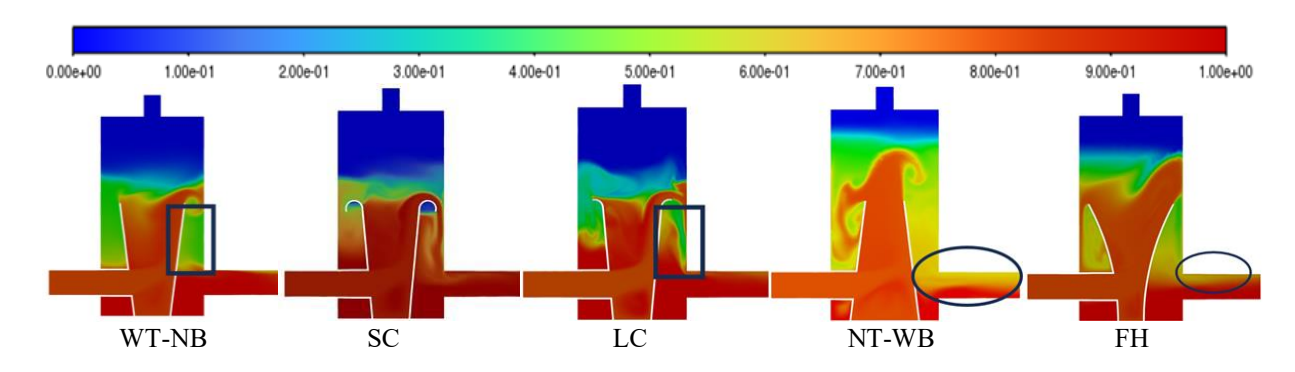


Fig. 18 Contour map of liquid phase distribution of different structures

evaluating performance as follows: separation efficiency > pressure drop at the bottom flow outlet > pressure drop at the gas phase outlet. Consequently, the optimal inner cylinder length-to-diameter ratios were 375 mm in height and 150 mm in diameter.

# 4. STRUCTURAL OPTIMIZATION OF THE INNER CYLINDER

This section describes how the configuration of the inner cylinder and the outlet end was innovatively designed to enhance the separation efficiency of the gas—water separator, as shown in Fig. 17. The inner cylinder was designed in a truncated cone shape, with two configurations: wider at the top and narrower at the bottom (WT-NB), and vice versa (NT-WB). In addition, the outlet shape of the inner cylinder was adjusted to three forms: small curvature (SC), large curvature (LC), and a flared design (FH).

The flow field distributions of the five inner cylinder configurations were compared using the contour map illustrated in Fig. 18. The WT-NB structure reduced the liquid level through inclination, and the inner cylinder outlet end of the NT-WB and FH structures exhibited higher spouting heights. By contrast, the bottom flow outlet of the NT-WB contained less of the liquid phase and more gas. The LC structure demonstrated the smoothest fluid flow and the lowest spouting height at the outlet end of the inner cylinder. The SC and WT-NB structures had similar outlet heights, but the SC had a higher liquid phase concentration on the upper side of the bottom flow outlet (in the black box).

The distribution of the liquid phase, illustrated by plotting the axial distribution of the liquid phase volume fraction for differing structures, was analyzed (Fig. 19).

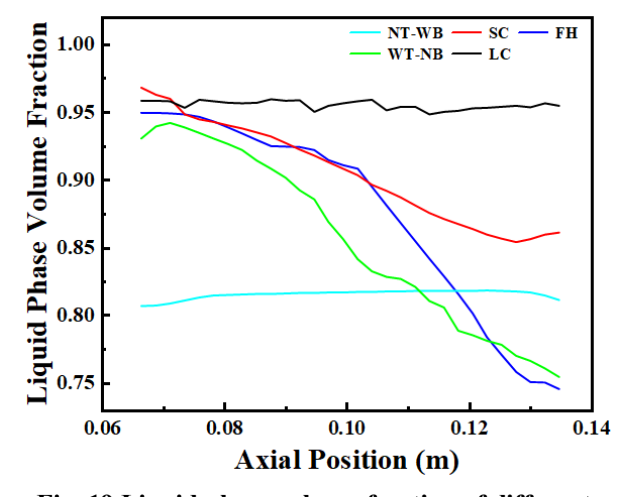


Fig. 19 Liquid phase volume fraction of different structures

The LC and NT-WB structures were distributed uniformly in the axial direction, exhibiting liquid phase volume fractions of approximately 95% and 80%, respectively. By contrast, the liquid phase volume fractions of the remaining three structures decreased with the increasing axial position, eventually reaching 75% for the FH and WT-NB types. The LC type effectively separated gas and liquid at the bottom outlet, improving overall performance.

Figure 20 shows the gas phase distribution in the axial direction, with the overall gas phase content increasing with height. Among the structures analyzed, the NT-WB type exhibited the highest gas-phase content at 0.35 m, and a decrease in the gas-phase content with height was observed. This indicated that the gas bubbles were clustered near the outlet end and did not rise. This was due to the narrow upper part of the structure and the high exit

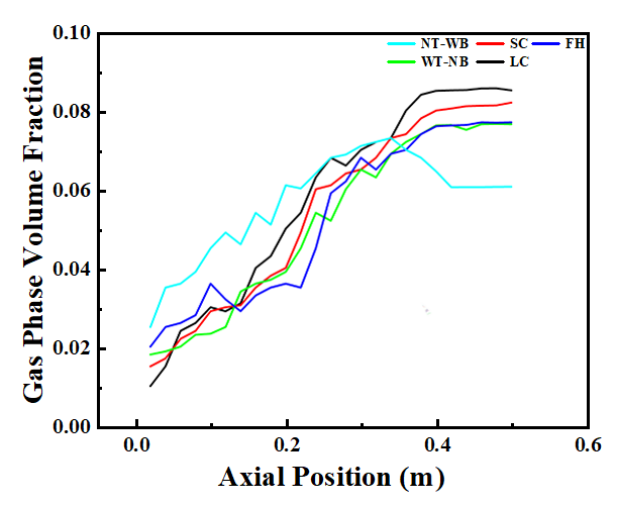


Fig. 20 Gas phase volume distribution in axial direction for different structures

velocity, for which inertia caused the gas to move downward with the water flow. The gas phase content at the bottom of the separator had to be kept as low as possible. In addition, the gas phase content at the bottom of all the structures except the NT-WB type was low, with the LC type exhibiting the lowest content, which indicated that it had the best separation effect. In addition, the gasphase volume fraction of the NT-WB-type structure was lower at the top, suggesting that it was not practical to hold up the gas.

### 4.1 Comparison of Velocity

Velocity variations inside the separator of different configurations were analyzed for the four cross-sections shown in Fig. 21. Section 4 in the figure corresponds to the plane through the inlet and outlet centerlines. Analyzing this section helped reveal the initial velocity distribution at the fluid entry and exit. Sections 1 and 2 were located near the inner-cylinder outlet, where the velocity magnitudes could indicate separation performance. Section 3 lay between these sections and represented a transitional stage, providing insights into the evolution of the velocity field.

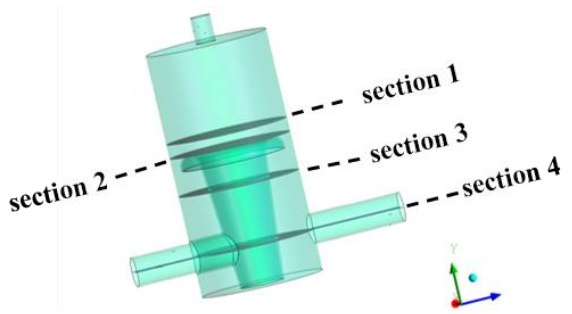


Fig. 21 Four cross-section locations

The axial velocity variation is illustrated in Fig. 22. Except for the WT-NB structure, the axial velocity at Section 1 was close to 0 m/s and stable, which indicated that the flow in this region was smooth. This was beneficial for the separation process in the initial stage.

The axial velocities of the LC, SC, and FH structures

were all above 0.4 m/s at the center of Section 4 of the inner cylinder and had approximately the same distribution. This suggests that the structure was effective in propelling bubbles toward the surface and thereby promoting their separation.

The two conical-table structures, WT-NB and NT-WB, had velocities of 0.3 m/s, which may have led to bubble retention and affected separation efficiency. The velocity was negative at the center of the inner cylinder in Section 3. By contrast, the axial velocity was higher near the ends of the inner cylinder, which may have affected the steady rise of the bubbles to the detriment of separation. The axial velocity at Section 2 could not be large to avoid an increase in turbulence intensity, which would be detrimental to the separation. Although the WT-NB type was more stable, the maximum axial velocity reached 0.6 m/s. The NT-WB type exhibited an unstable distribution, and the axial velocity reached a maximum of 1 m/s, which was detrimental to achieving separation.

As shown in Fig. 23, the tangential velocity varied considerably from section to section due to eddy currents, and the tangential velocity at the center of Section 4 was more significant than that at the other three sections. The tangential velocities of the LC structure at Sections 1–3 were higher than those for the other structures. This finding indicates that the configuration of the outlet end of the inner cylinder in a curved form enhanced the stability of the flow field, thereby mitigating flow separation and turbulence losses. The tangential velocity affected the speed of the separation process. The tangential velocities of the LC structure at Cross-Sections 1–3 were higher than those of the other structures, indicating that the LC structure was more advantageous in enhancing cyclonic strength and could provide greater separation power, which helped to improve the overall separation performance. Thus, it could be concluded that selecting a suitable inner cylinder structure (e.g., the LC structure) not only enhanced the cyclonic effect but also optimized the gas-water separation effect and improved the plant's efficiency.

As shown in Fig. 24, the radial velocity of each structure was 0 m/s near the wall, and the radial velocity increased further away from the wall and was distributed center-symmetrically. It was found that the radial velocities were generally small. None exceeded 0.6 m/s due to the weak effects of separation. The NT-WB-type structure had the opposite direction of radial velocity to the other structures at Section 4, indicating that it was most affected by the flow field and had a larger variation.

### 4.2 Comparison of Separation Efficiency and Pressure Dron

As shown in Fig. 25, among the five structures, the NT-WB and FH structures had lower separation efficiencies than the standard column structure, which did not provide an optimized effect. The LC structure showed an increase of 2.03% in the separation efficiency over that of the standard column structure. The WT-NB and SC structures also showed improvement in separation efficiency. The LC structure had the smallest pressure drop (Fig. 26) at the bottom flow outlet and consumed the

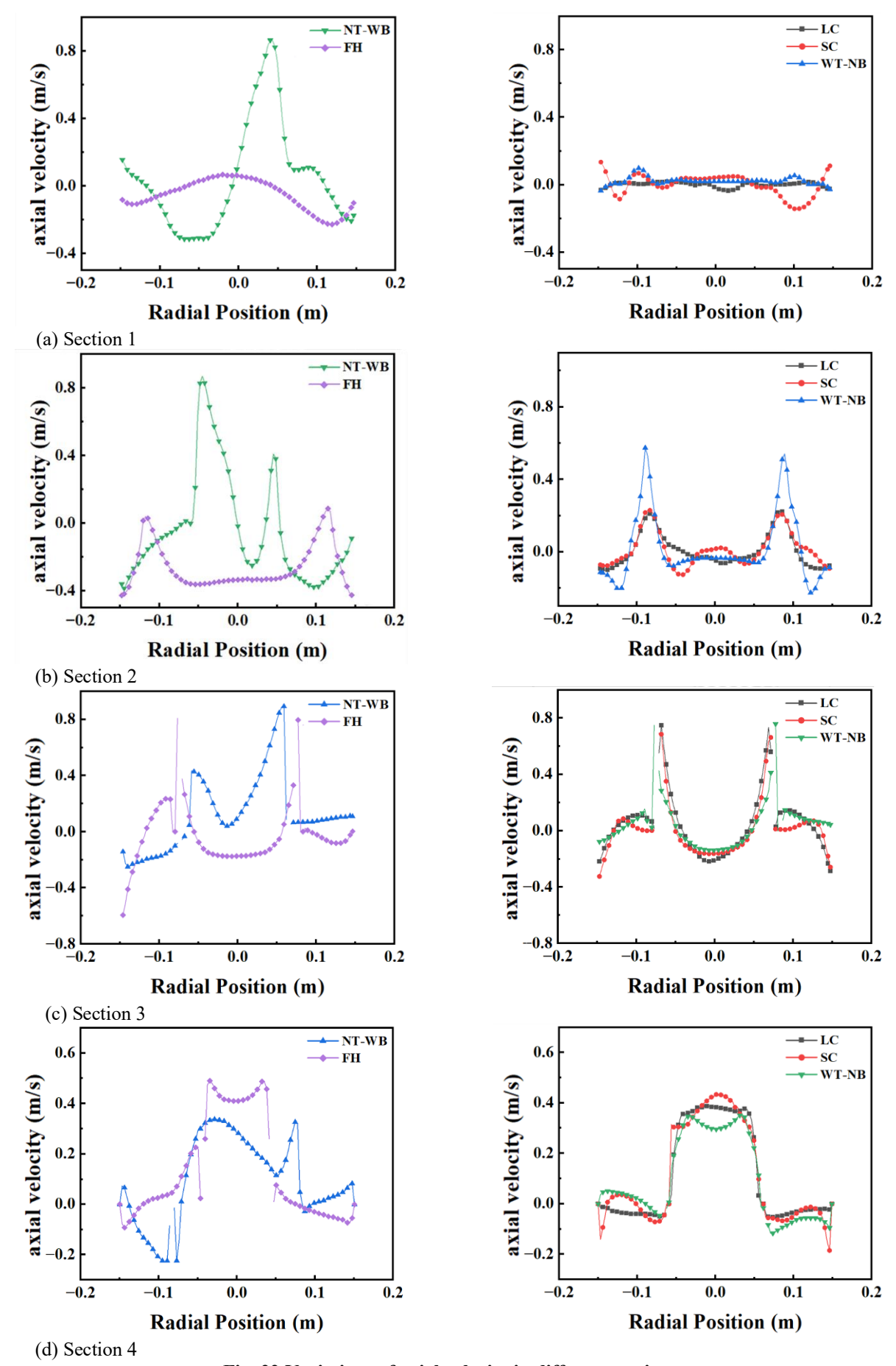


Fig. 22 Variations of axial velocity in different sections

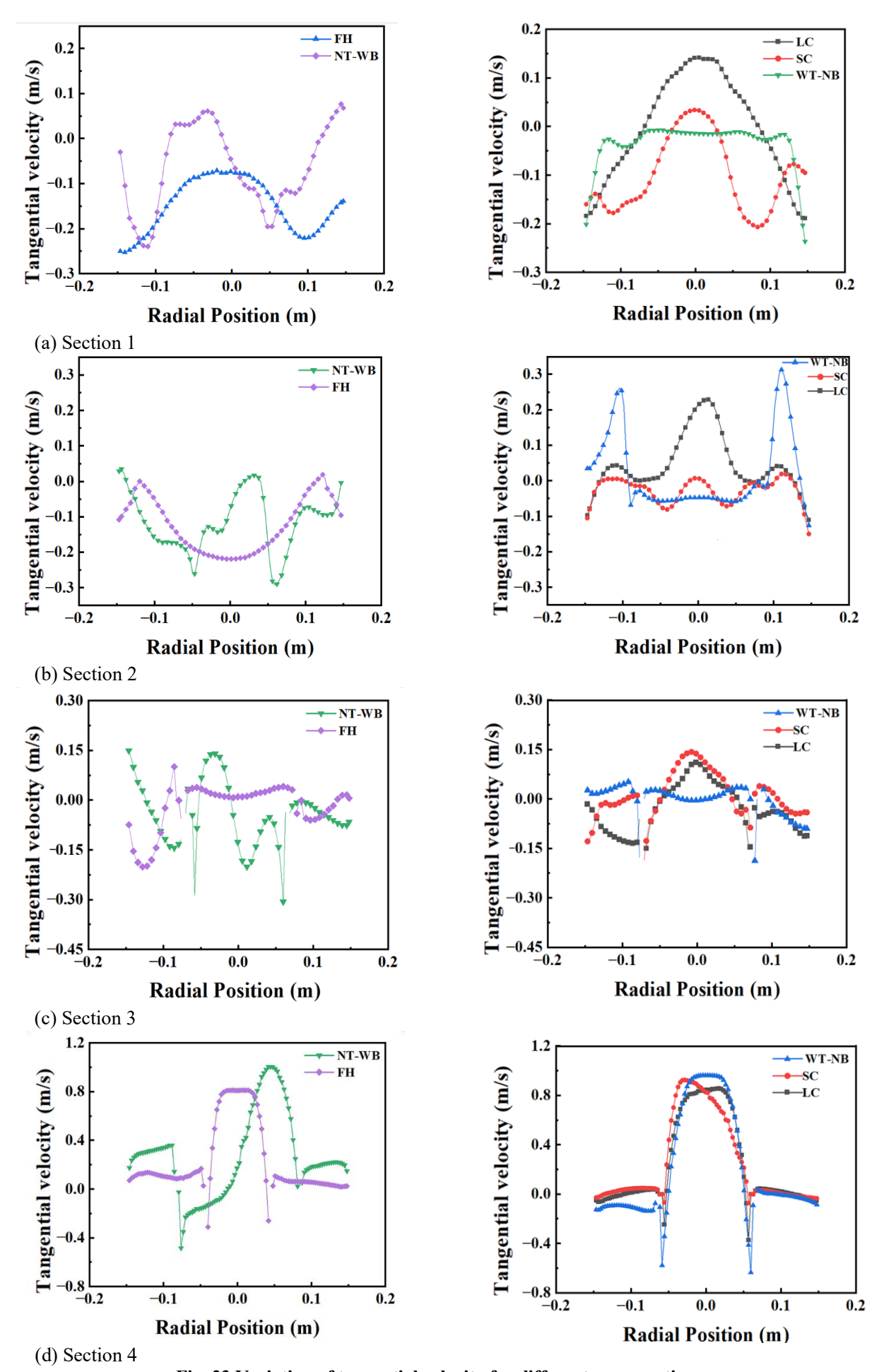


Fig. 23 Variation of tangential velocity for different cross-sections

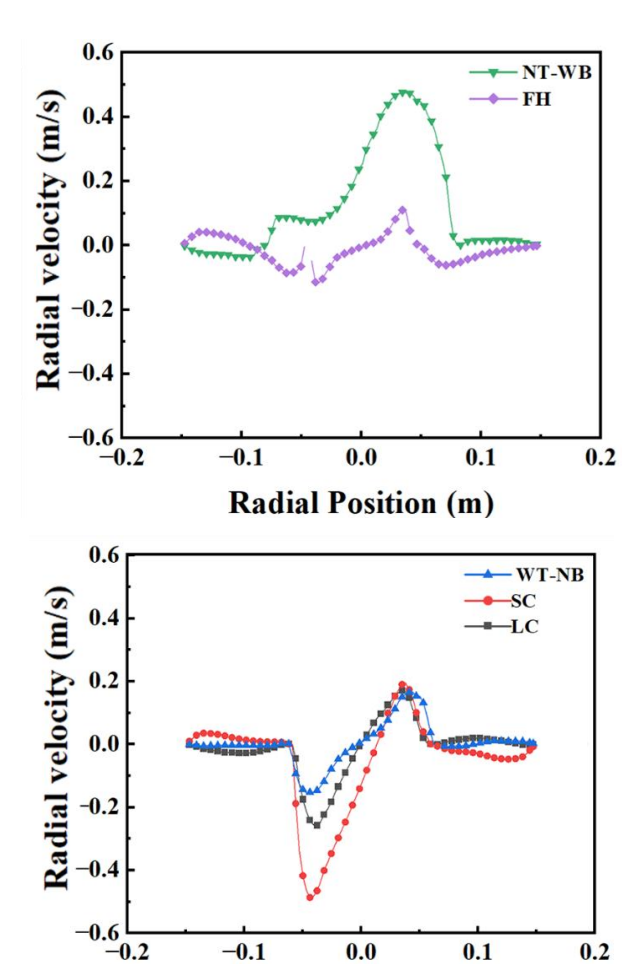
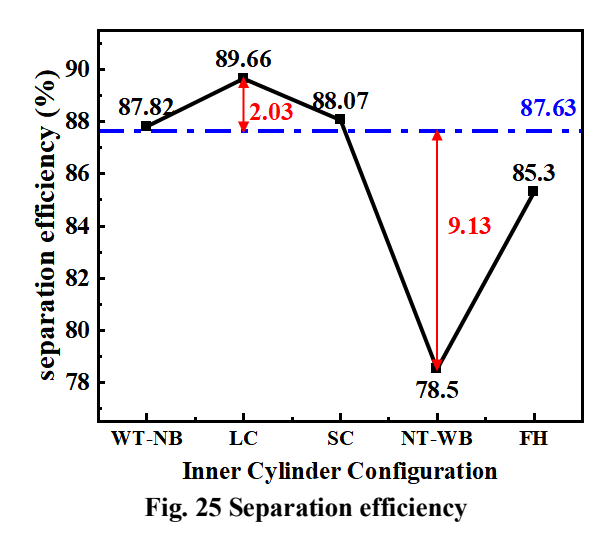


Fig. 24 Radial velocity variation in Section 4

Radial Position (m)



least amount of energy for separation. The LC structure was followed by the SC structure, indicating that the addition of a certain amount of curvature at the outlet end of the inner cylinder reduced the pressure loss inside the device.

The objective of optimizing the inner cylinder structure was to increase the unit's separation efficiency while reducing energy consumption. The LC structure satisfies both requirements, reducing the pressure loss by 208.66 Pa while increasing the separation efficiency by

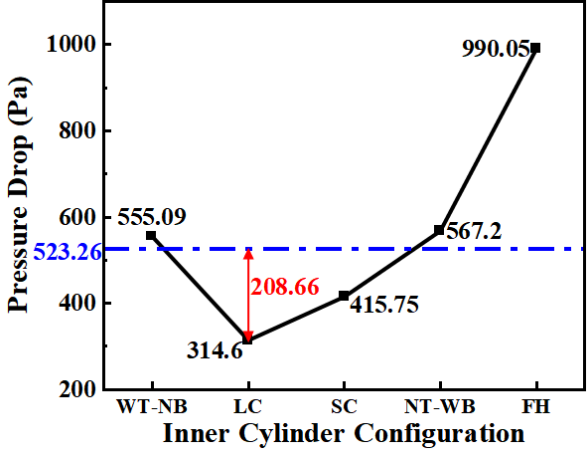


Fig. 26 Bottom flow outlet pressure drop

2.03%. Therefore, the LC structure was considered the best structure for the outlet end of the inner cylinder.

# 4.3 Optimization of Inner Cylinder Parameters Based on Orthogonal Testing

After determining the optimum separation effect of the structure of the LC, the inner cylinder structural parameters needed to be selected, so the next step was to further optimize the structural parameters through orthogonal tests.

This testing was used to examine the inner cylinder height, inner cylinder bottom diameter, and inner cylinder inclination, as well as the effects of these parameters on the separation efficiency of the gas—water separator, which was designed as a three-factor, four-level device. Table 3 displays the factor levels. According to the Randomization Principle, the factor level table ultimately formed 16 groups of combinations for the test.

Table 3 Factor level table

Factor	Height of inner cylinder (mm)	Diameter of the bottom of the inner cylinder (mm)	Inclination of inner cylinder (°)
1	320	100	87
2	330	110	85
3	340	120	83
4	350	130	81

According to the orthogonal test factor table, simulations were carried out using Fluent to obtain the separation efficiency for different parameter combinations, as shown in Table 4. Row K1 represents the sum of the simulated values for the first level of each factor, e.g., the first value of K1 represents the sum of the separation efficiencies for the corresponding tests (Nos. 1–4) for the height of the 320 mm inner cylinder. The terms k1, k2, k3, and k4 represent the mean values of K1, K2, K3, and K4.

Finally, according to the orthogonal test results, the order of factors influencing the separation efficiency was as follows: inner cylinder bottom diameter > inner cylinder inclination > inner cylinder height (R(B) > R(C) > R(A)). The highest separation efficiency of 91.42%, shown in Table 5, corresponds to the combination

**Table 4 Numerical simulation results** 

10	A (mm)	B (mm)	C (°)	Separation efficiency (%)
1	320	100	87	87.32
2	320	110	85	90.23
3	320	120	83	86.84
4	320	130	81	77.35
5	330	100	85	91.15
6	330	110	87	86.38
7	330	120	81	84.36
8	330	130	83	82.1
9	340	100	83	89.66
10	340	110	81	89.27
11	340	120	87	85.66
12	340	130	85	83.05
13	350	100	81	88.34
14	350	110	83	91.42
15	350	120	85	88.45
16	350	130	87	78.65

Table 5 Range analysis of separation efficiency

Level	A	В	С
K1	341.74	356.47	338.01
K2	343.9	357.30	352.88
K3	347.64	345.31	350.02
K4	346.86	321.15	339.32
k1	85.44	89.12	84.50
k2	86.00	89.33	88.32
k3	86.91	86.32	87.50
k4	86.72	80.28	84.83
R	1.47	9.05	3.72

A4B2C3: inner cylinder height of 350 mm, inner cylinder bottom diameter of 110 mm, and inclination of 83°. The k value reflects how each structural parameter affected the indicators. The factors influenced the separation efficiency in the order k3 > k4 > k2 > k1, and the B factors influenced the separation efficiency in the order k2 > k1. The order of the C factors influencing the separation efficiency was k2 > k3 > k4 > k1. The maximum K value for the three factors A, B, and C was k3, k2, and k2.

In the optimal scheme A3B2C2, the inner cylinder's height was 340 mm, the diameter of the bottom was 110 mm, and the inner cylinder's inclination was 83°. Further simulation validation of the model obtained from the orthogonal test showed that the separation efficiency could reach 91.86%.

### 5. RESULTS

In this study, we utilized numerical simulation to study a gas—water separator, design the structure, carry out simulation experiments, analyze the internal flow field characteristics, and then process the prototype to carry out cavitation testing. This testing verified that the separating device could effectively remove the air bubbles. Then, the effects of different inner cylinder length-to-diameter ratios on the separation performance were investigated, and the

separator structure was optimized by changing the shape of the inner cylinder and comparing the flow field and separation performance for different structures. The conclusions were as follows:

### (1) Velocity Component Interdependence

The three velocity vectors were interdependent in determining the separator's performance. The acceleration within the device was determined by the tangential velocity, which affected both the energy loss and the separation efficiency. The axial velocity drove the gas up, while the radial velocity played the smallest role.

## (2) Optimal Length-to-Diameter Ratio (2.5) Achieved 87.63% Separation Efficiency

The inner cylinder's length-to-diameter ratio for the inner cylinder affected the separation efficiency and pressure drop. The best separation was achieved when the inner cylinder length-to-diameter ratio was 2.5, with an efficiency of 87.63%.

### (3) LC Inner-Cylinder Shape Delivered Superior Performance

Different inner cylinder shapes optimized the separator performance, with the LC structure performing the best at the outlet end of the inner cylinder. This structure achieved a high separation efficiency of 89.66%, reducing the pressure drop by 208.66 Pa while increasing the separation efficiency by 2.03%.

## (4) Parameter Influence Ranking for LC Structure

The order of the degree of influence of the different parameters on the separation performance of the large curvature structure was as follows: inner cylinder bottom diameter > inner cylinder inclination > inner cylinder height. The optimum combination of the parameters was obtained as inner cylinder height of 340 mm, inner cylinder bottom diameter of 110 mm, and inner cylinder inclination of 83°, achieving a high separation efficiency of 91.86%.

### **CONFLICT OF INTEREST**

The authors declare that they have no conflicts to disclose.

### ACKNOWLEDGEMENTS

This study was supported by the National Natural Science Foundation of China (52479090). We thank LetPub (<a href="www.letpub.com.cn">www.letpub.com.cn</a>) for its linguistic assistance during the preparation of this manuscript.

#### **AUTHORS CONTRIBUTION**

Shuyi Dong: Conceptualization; Formal analysis; Software; Visualization; Writing—original draft. Jiegang Mou: Conceptualization; Methodology; Writing—review and editing. Bin Xiong: Conceptualization; Resources; Investigation; Supervision. Xiaohui Liu: Conceptualization; Methodology; Validation. Yuxin

Yang: Conceptualization; Data curation. Shengnan Fan: Conceptualization; Supervision. Zekun Liu: Conceptualization; Investigation.

#### REFERENCES

- Qiaorui, S., Asad, A., Minquan, L., Jianping, Y., Yuanyuan, G., Shouqi, Y., & Gerard, B. (2023). Assessment of cavitation noise in a centrifugal pump using acoustic finite element method and spherical cavity radiation theory. *Engineering Applications of Computational Fluid Mechanics*, 17(1). https://doi.org/10.1080/19942060.2023.2173302
- Ji, P., Qifan, D., Wenjie, W., Ju, S., & Wenjie, P. (2023). Investigation on energy dissipation mechanism in a double-suction centrifugal pump based on Rortex and enstrophy. *Engineering Applications of Computational Fluid Mechanics*, 17(1). https://doi.org/10.1080/19942060.2023.2261532
- Jiegang, M., Zicheng, Z., Yunqing, G., SHIZhengzan, & Shuihua, Z. (2020). Effect of Circular Non-Smooth Surface Blades onCavitation Characteristics of Centrifugal Pump. *JOURNAL OF SHANGHAI JIAO TONG UNIVERSITY*, 54(06), 577-583. <a href="https://doi.org/10.16183/j.cnki.jsjtu.2019.070">https://doi.org/10.16183/j.cnki.jsjtu.2019.070</a> (in Chinese)
- Guixuan, L., Peijian, Z., Gang, X., Jiegang, M., Yang, W., & Chengui, Z. (2023). Research on Cavitation State Recognition in Vortex Pump Based on Residual Neural Networks. *CHINESE JOURNAL OF HYDRODYNAMICS*, 38(06), 852-857. <a href="https://doi.org/10.16076/j.cnki.cjhd.2023.06.005">https://doi.org/10.16076/j.cnki.cjhd.2023.06.005</a> (in Chinese)
- Bo, G., Zhengchuan, Z., Junlian, Y., Rui, X., Ning, L., & Dezhong, W. (2024). Experimental study on the cavitation flow and the induced vibration characteristics of a mixed-flow water-jet pump. *JOURNAL OF VIBRATION AND SHOCK*, 43(02), 42-51. https://doi.org/10.13465/j.cnki.jvs.2024.02.005 (in

Chinese)

- Li, G., Ding, X., Wu, Y., Wang, S., Li, D., Yu, W., Wang, X., Zhu, Y., & Guo, Y. (2022). Liquid-vapor two-phase flow in centrifugal pump: Cavitation, mass transfer, and impeller structure optimization. *Vacuum*, 201, 111102. <a href="https://doi.org/https://doi.org/10.1016/j.vacuum.2022.111102">https://doi.org/https://doi.org/10.1016/j.vacuum.2022.111102</a>
- Gu, Y., Yu, L., Mou, J., Shi, Z., Yan, M., & Wu, D. (2022). Influence of circular non-smooth structure on cavitation damage characteristics of centrifugal pump. *Journal of the Brazilian Society of Mechanical Sciences and Engineering*, 44(4), 155.
- Lu, J., Luo, Z., Chen, Q., Liu, X., & Zhu, B. (2022). Study on pressure pulsation induced by cavitation at the tongue of the volute in a centrifugal pump. *Arabian Journal for Science and Engineering*, 47(12), 16033-16048.

- Tan, Y., Wu, G., Qiu, Y., Fan, H., & Wan, J. (2023). Fault diagnosis of a mixed-flow pump under cavitation condition based on deep learning techniques. *Frontiers in Energy Research*, 10, 1109214.
- Sakran, H. K., Abdul Aziz, M. S., Abdullah, M., & Khor, C. (2022). Effects of blade number on the centrifugal pump performance: a review. *Arabian Journal for Science and Engineering*, 47(7), 7945-7961.
- Ma, X., Luo, Y., Shi, J., & Xiong, H. (2022). Acoustic Emission Based Fault Detection of Substation Power Transformer. *Applied Sciences*, *12*(5), 2759.
- Xiaoqi, J., Shuaikang, Z., & Zuchao, Z. (2023). Experimental Prediction of Filtrate Pump's Critical Cavitation Point Based on Vibration Energy. *Iranian Journal of Science and Technology, Transactions of Mechanical Engineering*, 48(2), 615-627. https://doi.org/10.1007/S40997-023-00691-5
- Rudolf, B., Bernd, S., & Matevž, D. (2010). Unsteady Cavitation at the Tongue of the Volute of a Centrifugal Pump. *Journal of Fluids Engineering*, 132(6). https://doi.org/10.1115/1.4001570
- Yongbing, H., , Z. S., Jinyu, Q., Zhenkun, Z., Lian, S., Lei, L., & , M. L. (2020). Research on Cavitation Test Method of Pump. MECHANICAL & ELECTRICAL ENGINEERING TECHNOLOGY, 49(09), 76-77.
- Jorge, L., Redza, R., Nicolas, R., H, N. R., Eduardo, P., & Cem, S. (2024). Investigation of gas-bubbles separation from a liquid—gas mixture stream around a vertical 180° bend applied to gravity-driven separation using computing vision and computational fluid dynamics (CFD). *Experimental Thermal and Fluid Science*, 152, 111103-. https://doi.org/10.1016/J.EXPTHERMFLUSCI.202
- Zheng, C., Yang, W., Wang, G., Fan, G., Yan, C., Zeng, X., & Liu, A. (2019). Experimental study on a new type of separator for gas liquid separation. *Frontiers in Energy Research*, 7, 102. https://doi.org/10.3389/fenrg.2019.00102
- Jincheng, W., Dong, H., Shirui, L., Sheng, W., Weifeng, H., Mingrui, Z., & Sijie, C. (2023). Numerical Simulation of Vapor-liquid Separation Based on Cyclone Separator. *Machine Building & Automation*, 52(03), 101-105. <a href="https://doi.org/10.19344/j.cnki.issn1671-5276.2023.03.025">https://doi.org/10.19344/j.cnki.issn1671-5276.2023.03.025</a> (in Chinese)
- Hreiz, R., Gentric, C., & Midoux, N. (2011). Numerical investigation of swirling flow in cylindrical cyclones. *Chemical Engineering Research and Design*, 89(12), 2521-2539. <a href="https://doi.org/10.1016/j.cherd.2011.05.001">https://doi.org/10.1016/j.cherd.2011.05.001</a>
- Yan-ria, X., Xing-fu, S., Ya-zhou, W., You-riao, G., & Shu-min, L. (2012). Simulation Analysis of Hydrocyclone with Different Vortex Finders. Journal of East China University of Science and Technology (Natural Science Edition), 38(03), 271-276. https://doi.org/10.14135/j.cnki.1006-3080.2012.03.020

- Mao, Y., Chertovskih, R., & Cai, L. (2024). Numerical Study of the Gas–Solid Separation Performance of Axial Flow Cyclone Separators. *Inventions*, 9(2). <a href="https://doi.org/10.3390/inventions9020034">https://doi.org/10.3390/inventions9020034</a>
- He, F., Zhao, D., Wang, J., Huang, Y., & Liu, Q. (2022). Numerical Simulation Investigation of Vortex Finder Depth Effects on Flow Field and Performance of Desanding Mini-Hydrocyclones. *Journal of Marine Science and Engineering*, 10(11). https://doi.org/10.3390/jmse10111600
- Pandey, S., Saha, I., Prakash, O., Mukherjee, T., Iqbal, J., Roy, A. K.,...Brar, L. S. (2022). CFD Investigations of Cyclone Separators with Different Cone Heights and Shapes. *Applied Sciences*, 12(10). <a href="https://doi.org/10.3390/app12104904">https://doi.org/10.3390/app12104904</a>
- Zhi, Q., Ling, Z., Ling, B., A., E.-E. M., & Ramesh, A. (2024). Empirical and numerical advancements in gas-liquid separation technology: A review. *Geoenergy Science and Engineering*, 233, 212577. https://doi.org/10.1016/J.GEOEN.2023.212577
- Zhen, Z., Mengshan, S., & Xiang, L. (2022). Experimental study on the separation performance of a novel gas—liquid separator. *Advanced Powder Technology*, 33(11). https://doi.org/10.1016/J.APT.2022.103795

- Rui, Y., Ming-hu, J., Xi-cheng, C., & Qi, X. (2019). The Structure Design and Flowfield Analysis of GasLiquid Separation Cyclone. *Chemical Engineering & Machinery*, 46(01), 74-78. (in Chinese)
- Mengyang, W., Qiaolei, S., Ding, F., Yue, M., & Jiangang, W. (2023). Design and Analysis of Gas-Liquid Separator for Skid-mounted Wellhead Gas Recovery System. *CHINA PETROLEUM MACHINERY*, 51(10), 113-119. <a href="https://doi.org/10.16082/j.cnki.issn.1001-4578.2023.10.015">https://doi.org/10.16082/j.cnki.issn.1001-4578.2023.10.015</a> (in Chinese)
- Feiran, X., Jia, W., Jinming, C., Mengnan, S., Baoyu, W., & Yaohua, W. (2020). Structure Design and Simulation Analysis of Gas-water Separation Device for Diesel Engine. *Internal Combustion Engines*(05), 39-42. (in Chinese)
- Chunyu, M., Lei, X., Feng, L., Minghu, J., & Xinya, L. (2023). Significance Analysis of Structural Parameters of th Compact Gas-Liquid Hydrocyclone. **CHINA PETROLEUM** MACHINERY, 51(05), 86-93. https://doi.org/10.16082/j.cnki.issn.1001-4578.2023.05.012 (in Chinese)